Design of a Fully Pulley-Guided Wire-Driven Prismatic Tensegrity Robot: Friction Impact to Robot Payload Capacity

Azamat Yeshmukhametov and Koichi Koganezawa

***Abstract*—The tensegrity structure was initially created as a static structure, but it has gained significant attention among robotics researchers due to its benefits, including high payload capability, shock resistance, and resiliency. However, implementing tensegrity structures in robotics presents new technical challenges, primarily related to their wire-driven structure, such as wire-routing and wire-friction problems. Therefore, this research letter proposes a technical solution for the aforementioned problems. The main contribution of this research is the design of frictionless pulley-guided nodes. To validate the proposed concept, we conducted comparative experiments between a common tensegrity prototype and a pulley-guided prototype, evaluating wire tension distribution and payload capacity.**

I. Introduction

Tensegrity is composed of rigid compressed elements (bars) and flexible elastic elements (wire/cables), where rigid components of the tensegrity structure are connected indirectly via cables [1]. Such a compliant joint and lightweight design of tensegrity structure provide the following advantages over conventional robots; shock resistance, high payload capacity ratio, flexible structure, and capability of working in severe environments. The first term of "tensegrity" was coined by the American architect Buckminster Fuller in 1962 [2]. The tensegrity structure could be in different shapes; ball shape [3], [4], X-type (cross type) [5], bio-inspired [6] and prismatic shapes [7].

The remarkable structural capabilities of tensegrity robots have led to their widespread application in various fields of industry and research. One notable example is the use of icosahedra-shaped tensegrity structures, also known as ball-form tensegrity robots. These structures exhibit excellent absorption and resistance against external impacts, making them particularly attractive for space exploration missions [8]. Additionally, bio-inspired tensegrity robots have found utility in rescue operations, inspection tasks, and underwater [9]. The versatility and unique characteristics of tensegrity robots make them promising candidates for a wide range of applications in diverse industries and research fields.

This work was supported by the Science Committee of the Ministry of Education and Science of the Republic of Kazakhstan under Grant No. AP19574394

A. Yeshmukhametov is with the Department of Robotics and Mechatronics, School of Engineering and Digital Sciences, Nazarbayev University, Nur-Sultan, Kazakhstan. Email: {azamat.yeshmukhametov@nu.edu.kz

K. Koganezawa is with the Department of Mechanical Engineering, Tokai University, Hiratsuka, Kanagawa, Japan. Email: kogane@keyaki.cc.u-tokai.ac.jp

First tensegrity structures have served to inspire art, such as the biological structure of the human skeleton and muscles. By the principle of work, tensegrity structure imitates human anatomy structure where bones and muscles in biological composition provide great dexterity, maneuverability, and rigidity [10]. many researchers found tensegrity structure a curious topic for research and proposed many solutions in terms of mathematics, engineering, and architecture. Likewise, interest made tensegrity structure object for multidisciplinary research and collaboration [11]. Tensegrity structure found its first application in architecture, American Architect Fuller realized a sphere-shaped structure called Aspension Dome [12].

Moreover, after stationary application of tensegrity structure, researchers employed motors to manipulate tensegrity structures as a robot or kinetic sculptures [13]. Lightweight design and flexible structure presented the promising potential application of tensegrity structures in the industry. Motorizing of tensegrity structure imposed the first challenge related to form-finding [14]. The calculation of the initial equilibrium form of the tensegrity structure is known as "form-finding". The form-finding of the tensegrity robot is nontrivial because the form of the tensegrity should be symmetric in terms of wire tensions and robot posture. Finding the initial form of the robot after the moving is also an important task. Scholars and researchers proposed different approaches in this regard, such as genetic algorithms by [15], and new genetic algorithms with remarkably underlying graphs [16]. Furthermore, researchers proposed various methods of form-finding features for tensegrity structures, such as parametric approach [17], algebraic approach [18], algebraic model [19], minimal mass method [20], and complementary framework method [21].

Researchers have made significant contributions to the dynamic formulation of tensegrity structures in top academic journals. Tensegrity structure dynamics present distinct challenges compared to traditional mechanisms due to their flexible nature and hyper-redundancy. The dynamic formulation of a tensegrity robot takes into account various factors, including material properties such as elasticity and Young's modulus of its components [22]. An alternative dynamic formulation, proposed by Sultan, employs second-order ordinary differential equations, offering a simplified approach compared to partial differential equations [23]. However, the most widely recognized and influential dynamic formulation for tensegrity structures was introduced by Skelton et al. [24]. Skelton's formulation is based on nodes, bars, and string con-

nectivity matrices, providing a versatile framework applicable to different types of tensegrity structures. These dynamic formulations have significantly advanced our understanding of the intricate dynamics involved in tensegrity structures, paving the way for further exploration and the development of their capabilities. The publication of these findings in top academic journals has contributed to the dissemination of knowledge and the advancement of the field.

Driving tensegrity robot wires is also one of the most challenging issues because the tensegrity robot structure is unlike traditional manipulators where plenty of space for placing motors and sensors. Meanwhile in tensegrity structure only bars (struts) and wires. Therefore, the wire routing system would be complex and difficult to actuate, due to the friction effect between wire and robot rigid parts [25]. Wire-driven actuation presents notable challenges due to friction between wires and robot rigid parts. To address this issue, engineers and scholars have devised innovative solutions such as incorporating pulley idlers with grooves [26]. The use of pulley idlers helps in reducing friction, leading to smoother transmission mechanisms. Another critical aspect of wire-driven mechanisms is the proper routing and alignment of the wires. Precise wire alignment is vital to ensure efficient operation [27]. If there is a misalignment of the wire, it can result in the wire derailing from the pulley groove, leading to excessive torque consumption [28]. Hence, meticulous attention is required during the design and implementation phases to prevent such issues and optimize wire alignment for reliable actuation performance. By combining innovative solutions like pulley idlers with grooves and meticulous wire alignment, we can significantly enhance the effectiveness and efficiency of wire-driven actuation systems. These advancements hold promising potential for creating more robust and reliable robotic mechanisms that can overcome the challenges associated with friction and misalignment. Consequently, friction affects negatively the robot's accuracy, rigidity, and payload capacity [29]–[34].

This research paper introduces a novel design of pulley-guided nodes for tensegrity robots, along with wire routing schematics. The main focus is to address the challenges associated with wire-driven structures in tensegrity robotics. To validate the effectiveness of the proposed design, a series of experiments were conducted to assess the robot's payload capacity and wire tension distribution. These experiments serve as empirical evidence to support the proposed concept and highlight its potential benefits in practical applications. By presenting this new pulley-guided node design and wire routing schematics, this research paper contributes to advancing the field of tensegrity robotics and offers promising solutions to the technical challenges faced in wire-driven tensegrity structures.

One limitation of this research pertains to the mathematical formulation, which is specifically applicable to prismatic tensegrity structures. It is important to note that this formulation assumes a fixed base and a mobile top plate configuration.

A. Problem statement and related research

The wire-driven mechanism is one of the widespread methods of power or motion transmission in the robotics field. Motion transmission via cables allows the minimization of the robot's size and miniaturizes the robot's actuation system. However, wire-driven actuation and passive mechanisms without sufficient wire-routing schematics would suffer from derailing, wire slack, and friction between the wire and robot rigid parts [35]. Thus, one of the main tensegrity structure issues is the tension distribution of the driving wire. For instance, figure 1 demonstrates two different prismatic tensegrity robots with 4 layer structures, the left tensegrity structure nodes are simple non-pulley guided, and the right tensegrity nodes are built with pulley guided. As a result, the pulley-guided tensegrity structure is more symmetric and rigid. Likewise, the issue is more critical in the case driving of active wires to manipulate the robot to perform a certain task, in the case of 2 layer structure tension distribution is not significant, but over the 3 or more layers tension distribution would have a crucial impact on the whole robot structure [36].

B. Previous research

In previous research work, we have presented a novel kinematic and kinetic formulation for prismatic tensegrity structures [37]. Our study aimed to explore the influence of friction and wire tension distribution on the kinematics of robot nodes. Through experimental validation, we uncovered the significant impact of these factors. Additionally, we examined the dynamics of a six-bar tensegrity structure, providing further insights into the behavior of the robot [38].

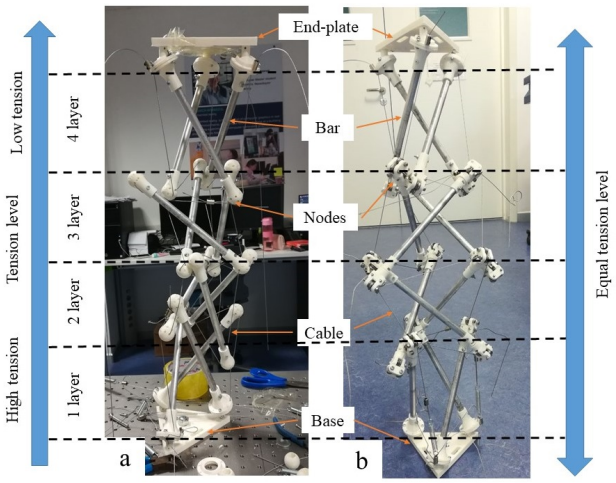

Fig. 1: 4 layered prismatic tensegrity structure with a) non-pulley guided node and b) pulley guided node design.

II. Design concept

A. General design

In this research, we present the design of a triangle prismatic tensegrity robot featuring pulley-guided wire-driven actuation. Two distinct models of the robot are considered, as illustrated in Fig. 1 (4 layers with 12 bars) and Fig. 2 (2 layers with 6 rods), respectively. These models exhibit key differences, which we will explain in detail. The nodes in the robot are categorized into three parts: base nodes, mid nodes, and end nodes. Base nodes are designed with two degrees of freedom (DOF) universal joint, while mid nodes incorporate wire guiding pulleys. The pulleys are fabricated using 3D printing techniques, except for the ball bearings component within the idle pulleys. End nodes are designed with a spherical joint, providing three DOF. To enable actuation, the robot employs three active wires, each controlled by an individual motor. Additionally, three passive wires are equipped, which are stretched by individual extension springs. The pretension of these springs is adjustable. The structure also includes a saddle wire, which serves to maintain static balance by utilizing gravitational force. The combination of these design elements and actuation mechanisms allows for the controlled and coordinated movement of the tensegrity robot. The unique features and capabilities of the proposed design make it a promising platform for various applications, including those requiring dexterity, adaptability, and robustness.

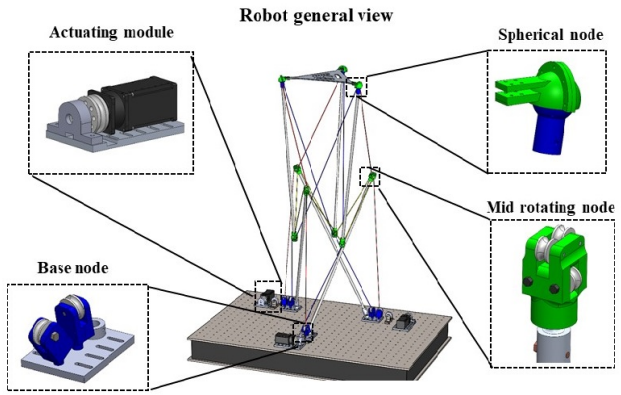

Fig. 2: Tensegrity robot general CAD design

B. Base part design

The robot base consists of three base nodes (n_{01}, n_{02}, and n_{03}, as shown in Figure 3), along with actuating modules. These base nodes are designed specifically with a spherical joint, which ensures proper self-alignment of the pulley for effective wire guiding during motion. One of the key challenges in wire-driven mechanisms is to prevent wire derailing and slackening.

Wire derailing occurs when the wire goes out of the pulley grooves, resulting in a cracking noise and potentially damaging the driving units. To address this issue, we have developed a spherical base node that inherits three degrees of freedom from a spherical joint, as depicted in Figure 4. This spherical node incorporates a self-alignment mechanism for the wire routing angle, enabling the pulley to maintain a right angle to the wire, thus preventing derailing.

For the driving motor, we have employed Dynamixel H54-200-S500 motors equipped with embedded encoders and torque sensors. These motors provide the necessary driving force and enable precise control and feedback during robot operation.

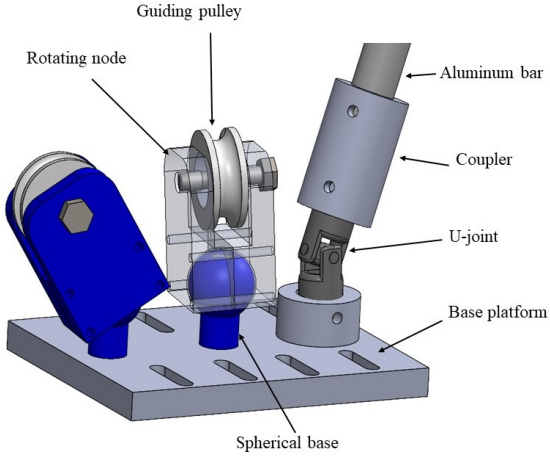

Fig. 3: Base node CAD design

In the previous prototype, we conducted tests using a simple joint with only one degree of freedom instead of the spherical joint. However, during these tests, we encountered issues such as wire derailing and an increase in friction, as depicted in Figure 4. These problems highlighted the limitations of the simple joint design and emphasized the need for a more advanced solution.

By transitioning to the spherical joint design in our current prototype, we have successfully addressed these challenges. The spherical joint not only prevents wire derailing but also reduces friction, ensuring smooth and efficient wire guiding. This improvement demonstrates the significance of utilizing advanced joint mechanisms in wire-driven systems, emphasizing the importance of our research findings.

C. Middle part design

The design of the middle part node, as illustrated in Figure 5, is a crucial aspect of our research. In order to achieve rotational functionality, we have implemented a full pulley-guided design for this node. Similar to the base part nodes, the middle part node also incorporates a self-aligned feature. The incorporation of a self-alignment feature has been made feasible by securing the linear bearing to the interior of the mid-node part, which then moves along the fixed linear guide shaft attached to the coupler. In the past, ball bearings were employed for similar purposes; however, they were unable to withstand the tension forces generated during motion. By

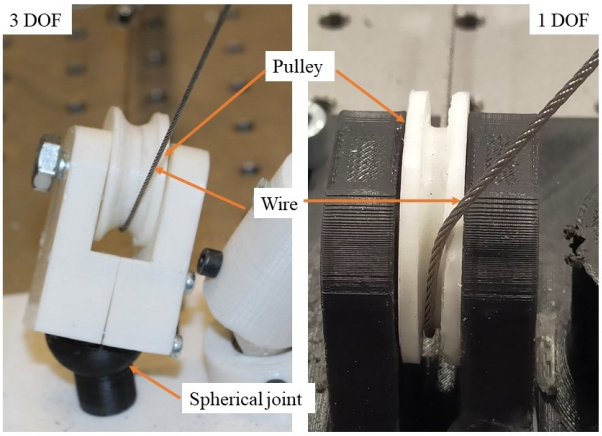

Fig. 4: Fabricated base nodes with 3 DOF (new model) and 1 DOF (previous model)

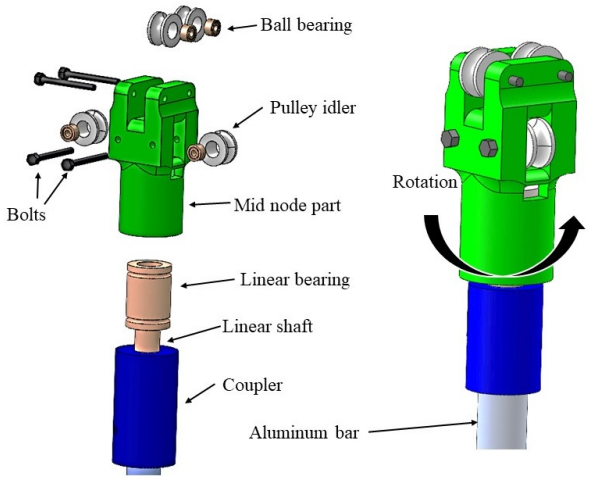

Fig. 5: Mid node CAD and fabricated design

contrast, the linear bearing offers significant advantages due to its larger contact area, allowing it to efficiently handle tension forces while ensuring smoother motion along the linear guide shaft. This improvement in the bearing system promises to enhance the overall performance and reliability of the mechanism.

The middle nodes, represented by n_{11}, n_{12}, n_{13}, n_{1a}, n_{1b}, and n_{1c} in Figure 7, serve as joints through which both passive and active wires are routed. To ensure smooth wire movement, we have integrated ball bearings within all pulleys, as depicted in Figure 5. This inclusion of ball bearings enhances the sliding performance of the wires, minimizing friction and enabling efficient operation of the system. By incorporating these design elements into the middle part node, we have achieved a robust and reliable mechanism that facilitates proper wire routing and smooth wire sliding. The utilization of ball bearings in the pulleys significantly contributes to the overall performance and functionality of our system, as detailed in this research.

D. Upper node design

The upper plate of the tensegrity robot comprises a triangular aluminum plate and spherical nodes. The spherical nodes consist of two components: a spherical joint for wire connection and spherical caps that cover the joint and connect it to the aluminum end plate (Figure 6). These components ensure stability and integrity within the robot's structure.

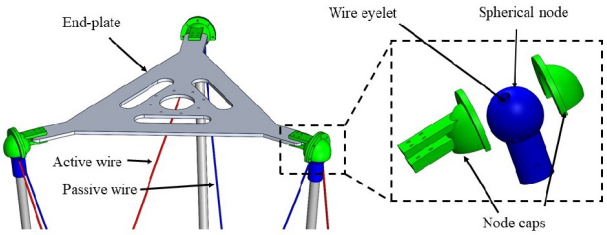

Fig. 6: Tensegrity robot upper node design

III. Wire Tension Analysis

Measuring wire tension on tensegrity structure is empirical proof of the proposed concept. Tension distribution is one of the critical features for tensegrity structure, uneven distribution of tension in different layers might cause undesired behavior, low rigidity in part, and inaccuracy in motion.

Tension distribution fully depends on wire routing schematics, so the routing of wires should be designed so as to make friction as small as possible. For this purpose, we measured tension distribution along the saddle wire by equipping six tension sensors as shown in figure 7.

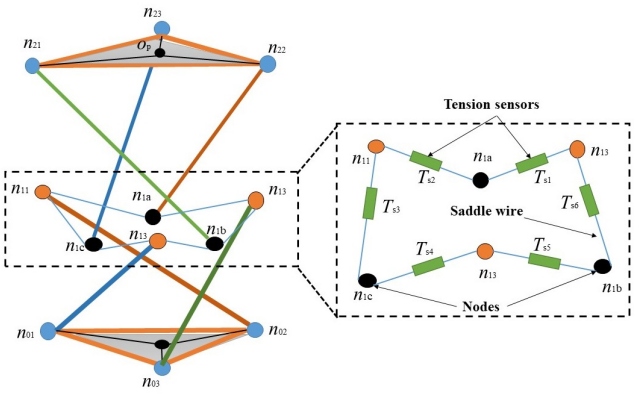

Fig. 7: Tension distribution experiment methodology

Flintec Y1 sensor (see figure 8 was used to measure the tension value between the nodes on states of standby and motion. This experiment proves the efficiency of pulley-guided node design over non-pulley guided ones (figure 8. Figure 9 shows sensor output on the saddle wire of a non-pulley guided tensegrity robot. We observed uneven tension distribution, especially during moving. Sharp angles between wire and node hamper the wire slide along nodes which

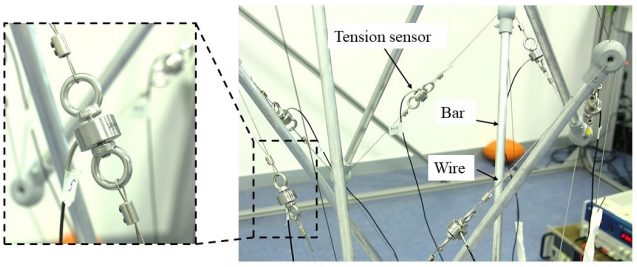

Fig. 8: Experimental setup on tension distribution

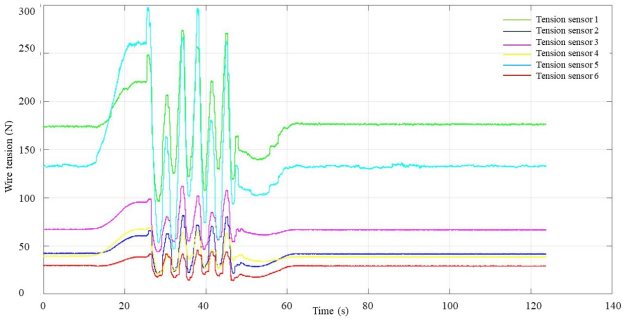

Fig. 9: Non-pulley guided tensegrity structure wire tension value

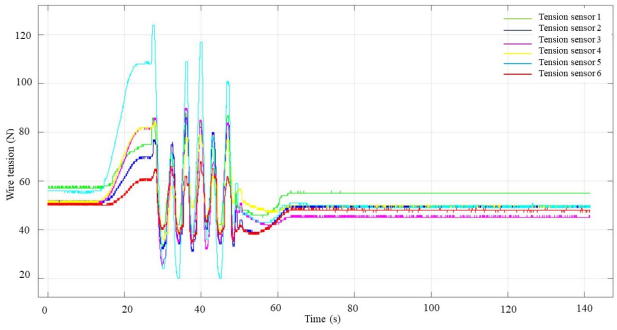

Fig. 10: Pulley guided tensegrity structure wire tension value

yielded a fairly uneven distribution of wire tension. While pulley pulley-guided node demonstrates much better tension distribution of each segment of the wire on saddle wire shows a similar value (figure 10). Figure 11 demonstrates

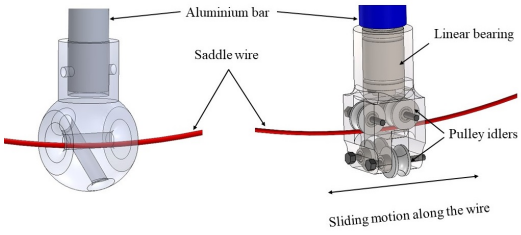

Fig. 11: Node displacement schematics along the saddle wire

the wire displacement schematics of the saddle wire. The pulley-guided nodes provide a constant distance between nodes and smooth sliding motion along the saddle wire. Likewise, the effect is clearly seen in figure 12, which demonstrates the motion timeline of the tensegrity robot in sinusoidal motion. To prove the concept, we used marker tape to capture wire/node displacement along the saddle wire, and based on the obtained result the pulley-guided node showed a sliding motion up to 25mm, while the non-pulley-guided node demonstrated no displacement.

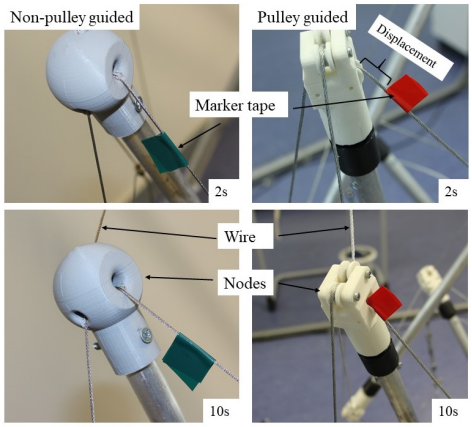

Fig. 12: Node displacement timeline

IV. Static Equilibrium Formulation

The stiffness formulation of the robot is considered only for the middle nodes of the robot, those nodes along the saddle wire. Exactly middle nodes have a critical impact on the robot during the motion and finding the form. Stiffness formulation is based on torque vector. The torque vector in the proposed prototype defines by the direction of gravitational force (figure 13.

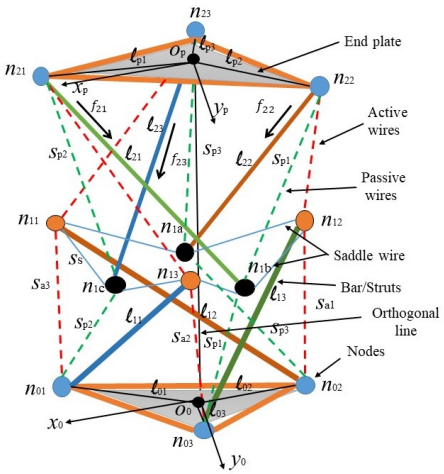

Fig. 13: General structure notation of tensegrity robot

A. Node Positions

As a preliminary step, we introduce the rotation matrices for an angle θ around the x, y, and z axes of a generic right-handed reference frame as

$$e^{\hat{i}\theta}=\begin{pmatrix}1 & 0 & 0\\ 0 & cos(\theta) & -sin(\theta)\\ 0 & sin(\theta) & cos(\theta)\end{pmatrix} e^{\hat{j}\theta}=\begin{pmatrix}cos(\theta) & 0 & sin(\theta)\\ 0 & 1 & 0\\ -sin(\theta) & 0 & cos(\theta)\end{pmatrix}$$

$$\mathrm{e}^{\hat{k}\theta}=\begin{pmatrix}cos(\theta) & sin(\theta) & 0\\ -sin(\theta) & cos(\theta) & 0\\ 0 & 0 & 1\end{pmatrix} \quad (1)$$

where $\hat{i}$, $\hat{j}$ and $\hat{k}$ are the skew-symmetrix matrices composed by elements of unit vectors i,j and k respectively. Specifically, we will use two reference frames, both shown in Fig. 13: the first, namely $O_0 - x_0y_0z_0$, is a fixed frame with origin at the center of the base plate while the second, $O_p - x_py_pz_p$ is a moving frame attached to the top plate, with its origin at the center of this plate.

We will now detail how each node position of our prismatic tensegrity robot is obtained in the $O_0 - x_0y_0z_0$ frame. We can write the nodes in the base plate as The position of the nodes is calculated as,

$$n_{0i} = e^{\hat{k}(\frac{2\pi(i-1)}{3})}(l_{0i} \quad 0 \quad 0)^T, (i = 1, 2, 3) \quad (2)$$

$$n_{1i} = n_{0,p(i)} + e^{\hat{i}\theta_{0p(i)x}} e^{\hat{j}\theta_{0p(i)y}} (0 \quad 0 \quad l_{1p(i)})^T \quad (3)$$

where $p(i) = 2\delta(i-1) + 3\delta(i-2) + \delta(i-3), i = (1, 2, 3)$ where $\delta_{i,1}$, $\delta_{i,2}$, and $\delta_{i,3}$ with the Kronecker delta function $\delta(*)$. θ_{0ix} and θ_{0iy} are two rotation angles of the universal joint at the n_{0i} (i=1,2,3) node.

Three nodes of the top triangle plate are assumed to take positions such that,

$$n_{2i} = n_{up} + e^{\hat{i}\phi_{px}} e^{\hat{j}\phi_{py}} e^{\hat{k}\phi(pz+rpi)} (l_{pi} \quad 0 \quad 0)^T, \quad (4)$$

$(i = 1, 2, 3)$ and $(rp_1 = -\frac{\pi}{3}, rp_2 = \pi, rp_3 = \frac{\pi}{3})$ where, $\mathrm{n}_{up} = (u_{px} \quad u_{py} \quad u_{pz})^T$ is the position of the upper plate origin O_p, and $\phi_{px}, \phi_{py}, \phi_{pz}$ are tilting angle of the top-plate with respect to the base frame.

$$n_{1\rho} = n_{2<\rho>} - e^{\hat{i}\phi_{px}} e^{\hat{j}\phi_{py}} e^{\hat{k}\phi_{pz}} e^{\hat{i}\theta_{2<\rho>x}} e^{\hat{j}\theta_{2<\rho>y}} \begin{pmatrix}0\\0\\l_{2<\rho>,}\end{pmatrix},$$

$(\rho = a, b, c)$, and $(< a >= 3, < b >= 1, < c >= 2)$ (5)

where, $\theta_{2<\rho>x}$ and $\theta_{2<\rho>y}$ are two rotation angles of the universal joint at the $n_{2<\rho>}(\rho = a, b, c)$ node.

Note: The notation $\langle x \rangle$ represents the average or expected value of variable x. where, $\theta_{2<\rho>x}$ and $\theta_{2<\rho>y}$ are two rotation angles of the universal joint at the $n_{2<\rho>}(\rho = a, b, c)$ node. Torque vector applied at nodes n_{01}, n_{02} and n_{03}:

$$T_{01} = (n_{13} - n_{01}) \times (s_{a2}(\overbrace{(n_{21} - n_{13})} + \overbrace{(n_{03} - n_{13})}) + \frac{m_L g}{2}) \quad (6)$$

$$T_{02} = (n_{11} - n_{02}) \times (s_{a3}(\overbrace{(n_{23} - n_{11})} + \overbrace{(n_{01} - n_{11})}) + \frac{m_L g}{2}) \quad (7)$$

$$T_{03} = (n_{12} - n_{03}) \times (s_{a1}(\overbrace{(n_{22} - n_{12})} + \overbrace{(n_{02} - n_{12})}) + \frac{m_L g}{2}) \quad (8)$$

where, $\overbrace{(n_{22} - n_{12})} = n_{22} - n_{12}/|n_{22} - n_{12}|$, etc. m_L is the mass of the rod and $g = (0, 0, -9.80665)^T$. Tension due to friction is assumed to load at every six nodes on the saddle wire, which is assumed to be in parallel with the angle between the rod and wire direction. Figure 14 Tensegrity robot torque vector notation. Torque vector applied nodes at n_{21}, n_{22}, n_{23}:

$$T_{21} = (n_{1b} - n_{21}) \times (s_{p1}(\overbrace{(n_{22} - n_{1b})} + \overbrace{(n_{03} - n_{1b})}) + \frac{m_L g}{2}) \quad (9)$$

$$T_{22} = (n_{1a} - n_{22}) \times (s_{p3}(\overbrace{(n_{23} - n_{1a})} + \overbrace{(n_{02} - n_{1a})}) + \frac{m_L g}{2}) \quad (10)$$

$$T_{23} = (n_{1c} - n_{23}) \times (s_{p2}(\overbrace{(n_{21} - n_{1c})} + \overbrace{(n_{01} - n_{1c})}) + \frac{m_L g}{2}) \quad (11)$$

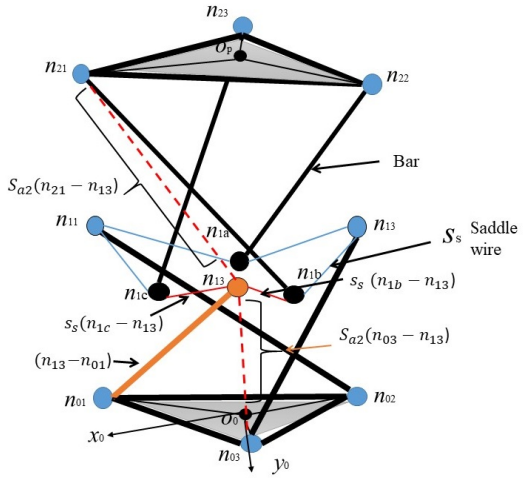

Fig. 14: Tensegrity robot vector torque notation

V. Payload Test

One notable advantage of tensegrity structures is their high potential for payload capacity. The FANUC robots datasheet [39] provides valuable information in this regard. The payload ratio of traditional serial manipulators can be calculated using the formula: $ratio$ = payload capacity/robot mass. Comparatively, the payload ratio of traditional manipulators typically falls within the range of 0.15-0.25. In contrast, tensegrity structures exhibit significantly higher payload

ratios, exceeding two times the traditional manipulators' payload ratio. This remarkable characteristic of tensegrity structures opens up new horizons of application for tensegrity robots.

TABLE I: Comparison table of pulley guided (PGTR) and non-pulley guided tensegrity robot (NGTR)

Parameter	PGTR	NGTR
Weight	6.2 kg	5.9 kg
Height	1.6 m	1.6 m
Bar length	1 m	1 m
Wire diameter	1 mm	1 mm
Active wire tension	60 N	60 N
Passive wire tension	60 N	60 N
Max. payload capacity	15 kg	12 kg
Weight-payload ratio	2.41	2.03

This research project presents the results of the payload experiment of two tensegrity prototypes; pulley-guided and non-pulley-guided tensegrity. In the case of the idle way, the robot moves easily without any buckling problems. However, in case carrying some load, the motion trajectory will be significantly different.

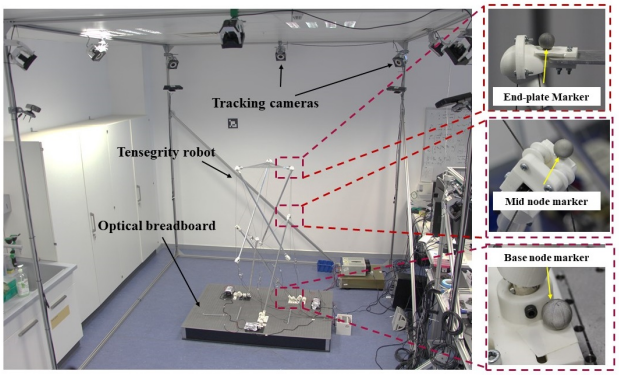

Fig. 15: Tensegrity robot experimental setup

In this experiment, we applied loads on the end plate of the robot to test robot motion trajectory precision. For both prototypes, we used the same trajectory and wire tension level and measured the trajectory by motion capture system Optitrack cameras (see fig 15). To follow the motion trajectory, the infrared emitting marker was fixed in the center of the plate. The experiment conducted four iterations with different levels of the load; no load and next iterations 3,6 and 9 kilograms respectively. The robot moves along linear reference first and does sinusoidal motion twice, then return back to the initial position.

The maximum payload capacity for non-pulley guided tensegrity made up 12 kg, while the pulley guided structure was able to manipulate up to 15 kg.

In this research experiment, the utilization of a pulley-guided node design (refer to Figure 17) significantly enhanced repeatability across various load capacities and motion trajectories. Notably, the motion trajectory is closely

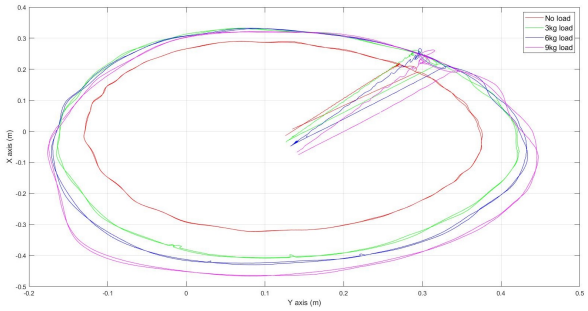

Fig. 16: Non-pulley guided tensegrity robot payload motion trajectory

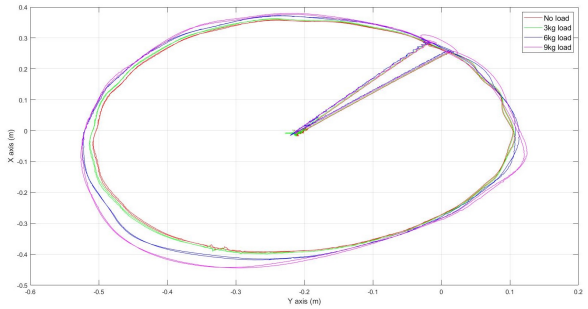

Fig. 17: Pulley guided tensegrity robot payload motion trajectory

aligned even in scenarios involving no load manipulation. Conversely, the non-pulley-guided node design (refer to Figure 16) experienced considerable challenges due to friction induced by conventional nodes. As a result, the motion trajectory exhibited diminished repeatability, especially when subjected to varying load capacities.

Similarly, the capabilities of robots extend to encompass pick and place operations within heavy industry and civil engineering sectors. The robot's hyper-redundant structure and lightweight design make it adept at operating in both confined and unstructured environments. Additionally, the absence of motors and sensors in its mobile components renders it ideal for deployment in the severe, dusty, and hazardous workspace.

VI. Conclusion and Future Plan

This research paper introduces a novel design concept for a pulley-guided tensegrity robot. An experimental analysis was conducted to assess the efficiency of the proposed design, focusing on tension distribution and payload testing. The results demonstrated that the prototype incorporating the pulley-guided design and nodes exhibited reduced friction effects and improved dexterity capabilities. The tension distribution experiment revealed the critical importance of shape conservation and form-finding features in tensegrity structures. In the absence of any load, the motorized tensegrity structure operated as expected; however, when subjected to weight, the distribution of tension played a significant role. To maintain the robot's shape, the nodes needed to slide along the saddle wire, a capability facilitated by the

pulley-guided prototype. Conversely, the non-pulley-guided prototype, affected by friction, was unable to provide smooth sliding along the saddle wire.

As part of our future research plan, this study aims to explore additional aspects of tensegrity robot features and capabilities. Specifically, our next objective is to validate the payload capacity and stiffness of prismatic tensegrity structures, particularly focusing on quadrangular shapes. The introduction of the novel pulley-guided node design enables the utilization of tensegrity structures not only as static frameworks but also for manipulation purposes. In light of this, we are also planning to conduct research on tensegrity robot manipulation and precision by leveraging the proposed frictionless nodes. By investigating these aspects, we aim to further enhance the understanding and potential applications of tensegrity robots in various domains.

REFERENCES

[1] K. Snelson, "The art of tensegrity," *International Journal of Space Structures*, vol. 27, no. 2-3, pp. 71–80, 2012. [Online]. Available: https://doi.org/10.1260/0266-3511.27.2-3.71

[2] R. E. Skelton and M. C. De Oliveira, *Tensegrity systems*. Springer, 2009, vol. 1.

[3] S. Mintchev, D. Zappetti, J. Willemin, and D. Floreano, "A soft robot for random exploration of terrestrial environments," in *2018 IEEE International Conference on Robotics and Automation (ICRA)*. IEEE Press, 2018, p. 7492–7497. [Online]. Available: https://doi.org/10.1109/ICRA.2018.8460667

[4] M. Vespignani, J. M. Friesen, V. SunSpiral, and J. Bruce, "Design of superball v2, a compliant tensegrity robot for absorbing large impacts," *2018 IEEE/RSJ International Conference on Intelligent Robots and Systems (IROS)*, pp. 2865–2871, 2018.

[5] Y. Liu, Q. Bi, X. Yue, J. Wu, B. Yang, and Y. Li, "A review on tensegrity structures-based robots," *Mechanism and Machine Theory*, vol. 168, p. 104571, 2022. [Online]. Available: https://www.sciencedirect.com/science/article/pii/S0094114X21003153

[6] B. Chen and H. Jiang, "Swimming performance of a tensegrity robotic fish," *Soft Robotics*, vol. 6, no. 4, pp. 520–531, 2019, pMID: 30985267. [Online]. Available: https://doi.org/10.1089/soro.2018.0079

[7] D. S. Shah, J. W. Booth, R. L. Baines, K. Wang, M. Vespignani, K. Bekris, and R. Kramer-Bottiglio, "Tensegrity robotics," *Soft Robotics*, vol. 9, no. 4, pp. 639–656, 2022, pMID: 34705572. [Online]. Available: https://doi.org/10.1089/soro.2020.0170

[8] A. P. Sabelhaus, J. Bruce, K. Caluwaerts, P. Manovi, R. F. Firoozi, S. Dobi, A. M. Agogino, and V. SunSpiral, "System design and locomotion of superball, an untethered tensegrity robot," in *2015 IEEE International Conference on Robotics and Automation (ICRA)*, 2015, pp. 2867–2873.

[9] E. Jung, V. Ly, N. Cessna, M. L. Ngo, D. Castro, V. SunSpiral, and M. Teodorescu, "Bio-inspired tensegrity flexural joints," in *2018 IEEE International Conference on Robotics and Automation (ICRA)*, 2018, pp. 5561–5566.

[10] S. M. Levin, "The tensegrity-truss as a model for spine mechanics: Biotensegrity," *Journal of Mechanics in Medicine and Biology*, vol. 02, pp. 375–388, 2002.

[11] A. Micheletti and P. Podio-Guidugli, "Seventy years of tensegrities (and counting)," *Archive of Applied Mechanics*, pp. 1–24, 2022.

[12] D. E. Ingber, "The architecture of life," *Scientific American*, vol. 278, no. 1, pp. 48–57, 1998.

[13] A. Hanaor, "Double-layer tensegrity grids as deployable structures," *International Journal of Space Structures*, vol. 8, no. 1-2, pp. 135–143, 1993.

[14] K. Song, F. Scarpa, and M. Schenk, "Form-finding of tessellated tensegrity structures," *Engineering Structures*, vol. 252, p. 113627, 2022. [Online]. Available: https://www.sciencedirect.com/science/article/pii/S014102962101717X

[15] X. Xu and Y. Luo, "Form-finding of nonregular tensegrities using a genetic algorithm," *Mechanics Research Communications*, vol. 37, no. 1, pp. 85–91, 2010.

[16] J. Rieffel, F. Valero-Cuevas, and H. Lipson, "Automated discovery and optimization of large irregular tensegrity structures," *Computers & Structures*, vol. 87, no. 5-6, pp. 368–379, 2009.

[17] K. A. Liapi and J. Kim, "A parametric approach to the design of vaulted tensegrity networks," *International Journal of Architectural Computing*, vol. 2, no. 2, pp. 245–262, 2004. [Online]. Available: https://doi.org/10.1260/1478077041518737

[18] D. Williamson, R. E. Skelton, and J. Han, "Equilibrium conditions of a tensegrity structure," *International Journal of Solids and Structures*, vol. 40, pp. 6347–6367, 2003.

[19] F. Maceri, M. Marino, and G. Vairo, "An operative algebraic formulation for the unilaterally-constrained mechanical problem of smart tensegrities," *International Journal of Solids and Structures*, vol. 51, no. 19, pp. 3333–3349, 2014. [Online]. Available: https://www.sciencedirect.com/science/article/pii/S0020768314002157

[20] R. Skelton, F. Fraternali, G. Carpentieri, and A. Micheletti, "Minimum mass design of tensegrity bridges with parametric architecture and multiscale complexity," *Mechanics Research Communications*, vol. 58, pp. 124–132, 2014.

[21] Z. Kan, H. Peng, and B. Chen, "Complementarity framework for nonlinear analysis of tensegrity structures with slack cables," *AIAA Journal*, vol. 56, no. 12, pp. 5013–5027, 2018.

[22] H. Murakami, "Static and dynamic analyses of tensegrity structures. part 1. nonlinear equations of motion," *International Journal of Solids and Structures*, vol. 38, no. 20, pp. 3599–3613, 2001. [Online]. Available: https://www.sciencedirect.com/science/article/pii/S0020768300002328

[23] C. Sultan, M. Corless, and R. E. Skelton, "Linear dynamics of tensegrity structures," *Engineering Structures*, vol. 24, no. 6, pp. 671–685, 2002. [Online]. Available: https://www.sciencedirect.com/science/article/pii/S0141029601001304

[24] R. Skelton, *Dynamic Systems Control: Linear Systems Analysis and Synthesis*. J. Wiley & Sons, 1988. [Online]. Available: https://books.google.kz/books?id=EcK2AAAACAAJ

[25] C. G. Manríquez-Padilla, O. A. Zavala-Pérez, G. I. Pérez-Soto, J. Rodríguez-Reséndiz, and K. A. Camarillo-Gómez, "Form-finding analysis of a class 2 tensegrity robot," *Applied Sciences*, vol. 9, no. 15, 2019. [Online]. Available: https://www.mdpi.com/2076-3417/9/15/2948

[26] J.-w. Suh and K.-y. Kim, "Harmonious cable actuation mechanism for soft robot joints using a pair of noncircular pulleys," *Journal of Mechanisms and Robotics*, vol. 10, no. 6, p. 061002, 2018.

[27] Y. Liu and F. Alambeigi, "Effect of external and internal loads on tension loss of tendon-driven continuum manipulators," *IEEE Robotics and Automation Letters*, vol. 6, no. 2, pp. 1606–1613, 2021.

[28] A. Yeshmukhametov and K. Koganezawa, "Design and development of wire-driven pulley guided continuum robot (wpgcr) arm and friction analysis," in *2022 IEEE/ASME International Conference on Advanced Intelligent Mechatronics (AIM)*. IEEE Press, 2022, p. 83–88. [Online]. Available: https://doi.org/10.1109/AIM52237.2022.9863244

[29] L. Zhang, B. Maurin, and R. Motro, "Form-finding of nonregular tensegrity systems," *Journal of Structural Engineering*, vol. 132, no. 9, pp. 1435–1440, 2006.

[30] M. Yamamoto, B. Gan, K. Fujita, and J. Kurokawa, "A genetic algorithm based form-finding for tensegrity structure," *Procedia Engineering*, vol. 14, pp. 2949–2956, 2011, the Proceedings of the Twelfth East Asia-Pacific Conference on Structural Engineering and Construction. [Online]. Available: https://www.sciencedirect.com/science/article/pii/S1877705811014482

[31] K. Koohestani, "Form-finding of tensegrity structures via genetic algorithm," *International Journal of Solids and Structures*, vol. 49, no. 5, pp. 739–747, 2012. [Online]. Available: https://www.sciencedirect.com/science/article/pii/S0020768311003970

[32] M. Pagitz and J. Mirats Tur, "Finite element based form-finding algorithm for tensegrity structures," *International Journal of Solids and Structures*, vol. 46, no. 17, pp. 3235–3240, 2009. [Online]. Available: https://www.sciencedirect.com/science/article/pii/S0020768309001802

[33] G. G. Estrada, H.-J. Bungartz, and C. Mohrdieck, "Numerical form-finding of tensegrity structures," *International Journal of Solids and Structures*, vol. 43, no. 22, pp. 6855–6868, 2006. [Online]. Available: https://www.sciencedirect.com/science/article/pii/S0020768306000448

[34] S. H. Juan and J. M. Mirats Tur, "Tensegrity frameworks: Static analysis review," *Mechanism and Machine Theory*, vol. 43, no. 7, pp. 859–881, 2008. [Online]. Available: https://www.sciencedirect.com/science/article/pii/S0094114X07001218

[35] A. N. Yeshmukhametov, K. Koganezawa, Z. Buribayev, Y. Amirgaliyev, and Y. Yamamoto, "Study on multi-section continuum robot wire-tension feedback control and load manipulability," *Industrial Robot: the international journal of robotics research and application*, vol. 47, no. 6, pp. 837–845, 2020.

[36] Z. Zhou, X. Zheng, Z. Chen, X. Wang, B. Liang, and Q. Wang, "Dynamics modeling and analysis of cable-driven segmented manipulator considering friction effects," *Mechanism and Machine Theory*, vol. 169, p. 104633, 2022. [Online]. Available: https://www.sciencedirect.com/science/article/pii/S0094114X21003669

[37] A. Yeshmukhametov and K. Koganezawa, "A simplified kinematics and kinetics formulation for prismatic tensegrity robots: Simulation and experiments," *Robotics*, vol. 12, no. 2, p. 56, 2023.

[38] D. Fadeyev, A. Zhakatayev, A. Kuzdeuov, and H. A. Varol, "Generalized dynamics of stacked tensegrity manipulators," *IEEE Access*, vol. 7, pp. 63 472–63 484, 2019.

[39] FANUC Corporation. (Year) Fanuc product catalog. [Online]. Available: https://www.fanuc.co.jp/en/product/catalog/index.html